Progress in Earth and Planetary Science
a SpringerOpen Journal

RESEARCH Open Access

Structure and properties of forsterite-$MgSiO_3$ liquid interface: molecular dynamics study

Fumiya Noritake* and Katsuyuki Kawamura

Abstract

The mechanical properties of partially molten rock, such as their permeabilities and viscosities, are important properties in geological processes. We performed molecular dynamics simulations in terms of structures and diffusivities in forsterite-$MgSiO_3$ liquid interfaces to obtain the nanoscale dynamic properties and structure of the interface. The characteristic structure of the forsterite-$MgSiO_3$ liquid interfaces was observed in the simulations. In the layered structure of the altered surfaces, Si-rich and Mg-rich layers exist alternately in the vicinity of the crystal-liquid interfaces. The layered structure might be formed by the strength difference between Si-O covalent bonds and Mg-O ionic bonds. The difference in the layered structure, indicated by the thickness of the $MgSiO_3$ liquid film, might be caused by the difference in degrees of freedom of the configuration in the liquid film. The two-dimensional diffusivity of oxygen atoms parallel to the interface is controlled by two factors. One factor is the thickness of the liquid film, which decreases oxygen diffusivity with decreasing film thickness. The other is the composition of the sliced layer, where oxygen diffusivity increases with increasing Mg/Si ratio. The effect of the crystal-liquid interface found in this study is negligible in texturally equilibrated rocks. However, the interface can affect the melt flow in deformed samples because a grain boundary melt film with a thickness of several nanometers exists stably in deformed partially molten rock.

Keywords: Solid-liquid interface; Molecular dynamics simulation; Forsterite; Silicate liquid

Background

Knowledge on viscosity and permeability of partially molten rocks is important for understanding volcanism and the thermal history of the earth. To understand the results obtained by experiments and to estimate physical properties in extreme conditions that are difficult to reproduce in laboratory experiments, it is necessary to know the local structure and the properties of silicate crystal-liquid interfaces. In particular, knowledge on the nanoscale structure and properties of silicate crystal-liquid interfaces might be useful in estimating the properties of rocks containing a small degree of melting. Hiraga et al. (2002) reported the presence of nanoscale melt films using high-resolution electron microscopy and energy dispersive X-ray profiling in scanning transmission electron microscopy. The properties of melt in such thin regions are considered to be different from properties in a bulk melt because of the effect of crystal surfaces. For instance, the lateral self-diffusivity of water to a crystal surface is different from a bulk surface in the case of a water-brucite surface (Sakuma et al. 2003), a water-muscovite mica surface (Sakuma and Kawamura 2009), and others. The dynamic property anomalies on solid-liquid interfaces affect the properties of bulk rock, e.g., permeability (Ichikawa et al. 2001).

Molecular dynamics simulations are widely used to investigate the physical properties and structures of crystals, liquids, gasses, and interfaces. In these simulations, we set the initial positions and velocities of all atoms; then, the atoms are forced to move according to given force fields under a proper ensemble. Molecular dynamics simulations are useful methods for investigating the nanoscale structure and properties because they give us the trajectory of each atom. In this study, the structure and properties of the forsterite-$MgSiO_3$ liquid interface are investigated by application of molecular dynamics simulations. It is essential to know the structure and physical properties of forsterite-$MgSiO_3$ liquid interfaces because forsterite is the liquidus mineral of primordial magmas.

* Correspondence: f.noritake@s.okayama-u.ac.jp
Graduate School of Environmental and Life Science, Okayama University, 3-1-1, Tsushimanaka, Kita-Ku, Okayama 700-8530, Japan

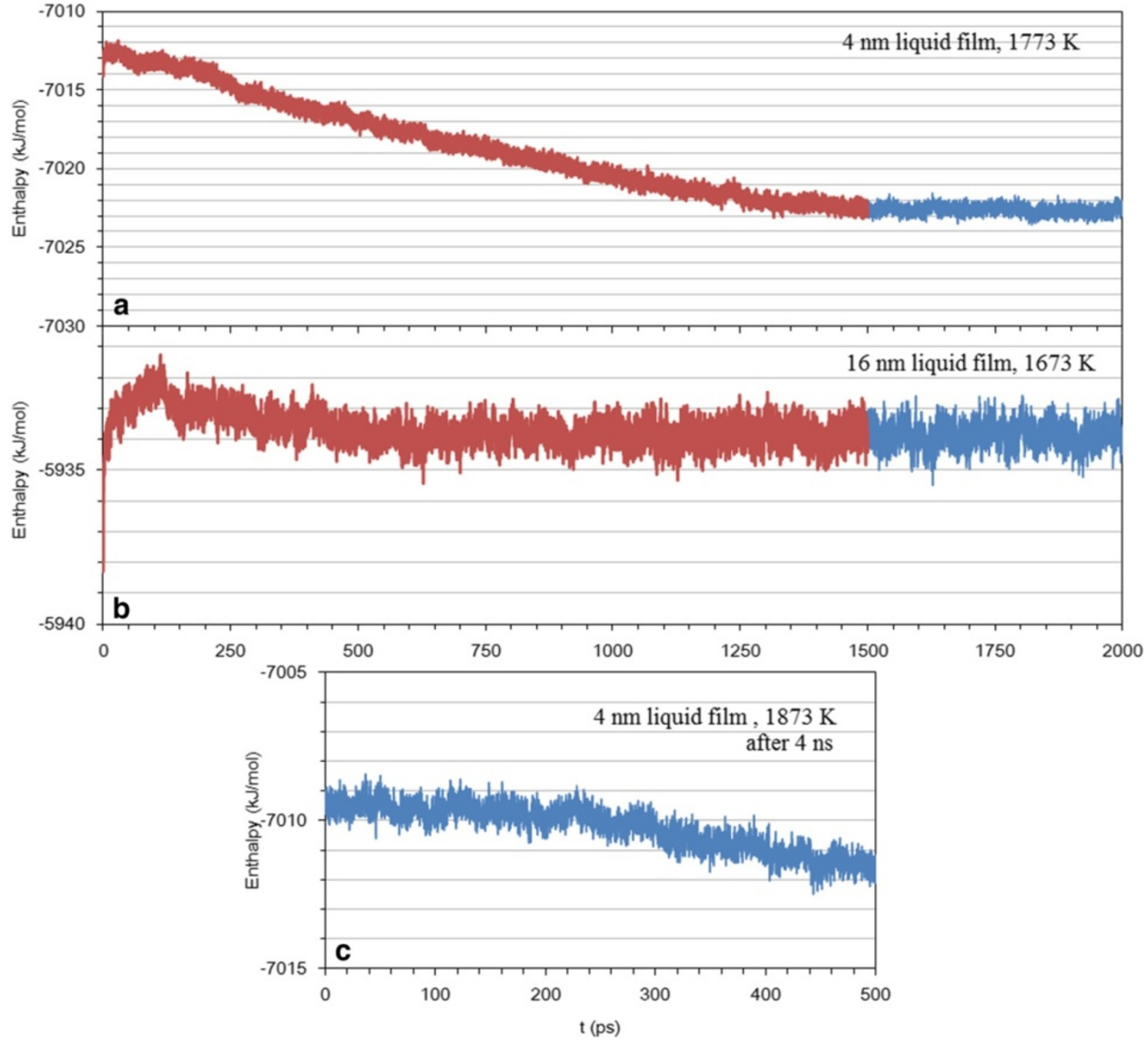

Figure 1 Plots of enthalpy of the simulated systems as a function of time. The enthalpy is plotted as molar enthalpy of **(a)** $Mg_{1.5459}Si_{1.0000}O_{3.5480}$, **(b)** $Mg_{1.2425}Si_{1.0000}O_{3.24345}$, and **(c)** $Mg_{1.5459}Si_{1.0000}O_{3.5480}$.

Methods

Molecular dynamics simulations were performed with the NPT ensemble at ambient pressure and various temperatures by application of the MXDORTO code (Sakuma and Kawamura 2009). The initial structure contains 21,440, 26,440, 43,440, and 63,440 atoms in which sheets of $MgSiO_3$ liquid consisting of 8,000, 15,000, 30,000, and 50,000 atoms (approximately 4-, 7-, 16-, and 28-nm thickness, respectively) are sandwiched between the (010) surfaces of forsterite. First, we simulated the equilibrated $MgSiO_3$ liquid film in a vacuum, starting with a randomly generated structure and randomly generated velocities of atoms through 0.5 ns (1,000,000 steps) at 1,973 K and

Table 1 Inter-atomic potential parameters

	Potential parameters and their values			
Atomic parameters	Q	a (Å)	b (Å)	c (kJ mol^{-1} Å^3)
Si	2.23607	0.99759	0.0830	0.000
O	−1.11803	1.81819	0.1539	27.400
Mg	1.11803	1.09881	0.0470	40.000
Pair parameters	D_1 (kJ mol^{-1})	β_1 (1/Å)	D_2 (kJ mol^{-1})	β_2 (1/Å)
Si-O	668,428	59.636	−105,335	45.514
Mg-O	28,960.0	5.0	−1,556.8	2.24
3-body parameters	f (kJ mol^{-1})	θ_0 (deg)	r_m (Å)	g_r (1/Å)
Si-O-Si	0.0006	147.0	0.170	168.0

Table 2 Comparison of lattice constants between MD simulations and experiments

	Forsterite		Enstatite	
	MD	Exp[a]	MD	Exp[c]
a (Å)	4.8709	4.7534	18.921	18.230
b (Å)	10.2820	10.1902	8.840	8.817
c (Å)	6.1249	5.9783	5.388	5.181
Density (g cm^{-3})	3.0467	3.2275	2.960	3.203
K_0 (GPa)	128	129[b]	95.0	95.8[d]
K'	5.69	4.2[b]	11.0	14.9[d]

MD, molecular dynamics; Exp, experiments. [a]Fujino et al. 1981. [b]Duffy et al. 1995. [c]Morimoto and Koto 1969. [d]Angel and Hugh-Jones 1994.

quenched to 300 K. Second, we simulated bulk forsterite with 13,440 atoms (11 × 5 × 8 unit cells of forsterite), starting with the given experimental crystal structure, which was obtained by an experiment (Fujino et al. 1981) and with randomly generated atom velocities; then, we cut along the (010) surface. Finally, we combined forsterite sheets along the (010) surface and an $MgSiO_3$ liquid film. We defined the *z*-axis perpendicularly to the (010) axis. Maintaining isobaric and isothermal conditions, we performed the relaxation up to 1.5 ns with a time step of 0.5 fs. Then, the statistical averages of the structure and physical properties were obtained from the velocities and coordinates of each atom in the simulations, through 500 ps. We confirmed that relaxation has been achieved by a plot of enthalpy versus time (Figure 1). The enthalpy of the system fluctuated around a constant value after 1.5 ns of relaxation (Figure 1a,b). The enthalpy of the system in the process of melting decreased, although 4 ns elapsed in the simulation (Figure 1c).

We imposed periodic boundary conditions in all directions. The Ewald summations were applied for evaluating the long-ranged Coulomb interactions. The pressure and temperature were kept constant at a given value through a scaling procedure. All the atoms were moved by application of the Verlet algorithm under a time interval of 0.5 fs. The function of the inter-atomic potential model was the same as that used in our previous work (Noritake et al. 2012):

$$U_{ij(rij)} = \frac{1}{4\pi\varepsilon_0}\frac{Z_i Z_j e^2}{r_{ij}} + f_0\left(b_i + b_j\right)\exp\left(\frac{a_i + a_j - r_{ij}}{b_i + b_j}\right) + \frac{c_i c_j}{r_{ij}^6} + D_{1ij}\exp\left(-\beta_{1ij} r_{ij}\right) + D_{2ij}\exp\left(-\beta_{2ij} r_{ij}\right) \quad (1)$$

where $U_{ij}(r_{ij})$ is the potential energy, ε_0 is the permittivity of a vacuum, Z_i is the effective charge of the *i*-th

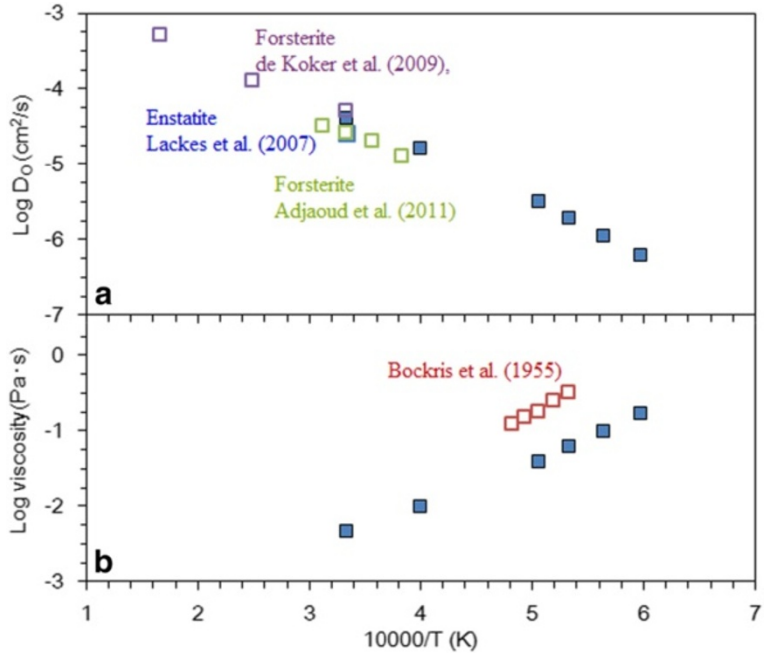

Figure 2 Comparisons of self-diffusion coefficients of oxygen and viscosities. (a) Comparison of diffusion coefficients of oxygen $MgSiO_3$ bulk liquid with other molecular dynamics studies. Closed squares indicate our study, and purple, green, and blue open squares indicate the data of forsterite liquid from de Koker et al. (2009), Adjaoud et al. (2011), and enstatite liquid by Lacks et al. (2007), respectively. **(b)** Comparison of calculated viscosities with experimental results. The experimental data are taken from Bockris et al. (1955). Viscosities are calculated using the Einstein-Stokes relation and the effective radius reported by Lacks et al. (2007).

atom, e is the elementary charge, r_{ij} is the distance between the i-th and j-th atoms, and f_0 is the constant 4.1865 kJ $Å^{-1}$ mol^{-1}. The values a_i, b_i, and c_i are the repulsion diameter, softness coefficient, and van der Waals coefficient of the i-th atom, respectively. The values D_{1ij}, β_{1ij}, D_{2ij}, and β_{2ij} are the parameters for the radial covalent bonds. The first term of this model gives the Coulomb potential, the second term gives the short-range repulsion, the third term is the van der Waals force, and the fourth and fifth terms are the radial part of the covalent bond. The three-body interactions between i, j, and k are represented as follows:

$$U_{kij} = -f\left[\cos\left\{2\left(\theta_{kij}-\theta_0\right)\right\}-1\right]\sqrt{k_{ij}k_{ik}} \tag{2}$$

$$k_{ij} = \frac{1}{\exp\left[g_r\left(r_{ij}-r_m\right)\right]-1} \tag{3}$$

where f is the force constant, θ_{kij} is the angle among the atoms k, i, and j, and θ_0, g_r, and r_m are parameters for adjusting the angular part of the covalent bonds. Atomic and pair parameters are given in Table 1. The potential parameters used in this study are the same as those used in Noritake et al. (2012) for silicon and oxygen atoms. We added new parameters for magnesium atoms empirically. We verified the potential parameters by calculating the lattice parameters and compressibility of forsterite and enstatite crystals (Table 2). The bulk modulus, K_0, and the

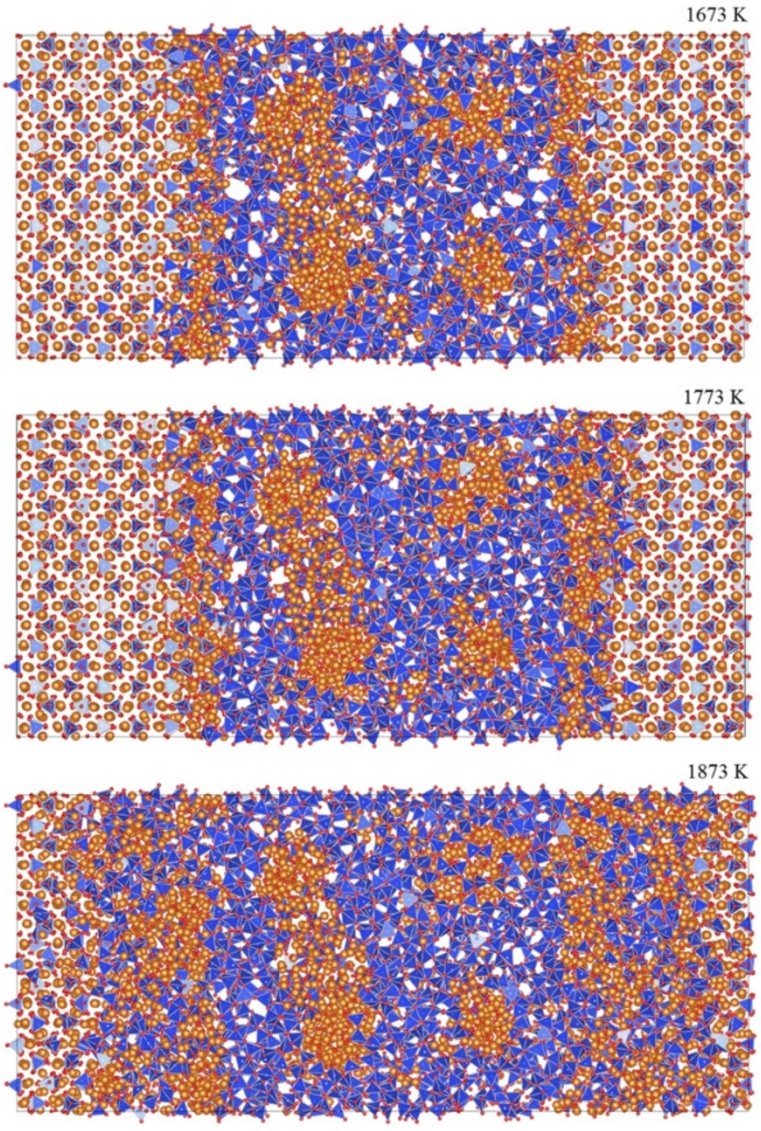

Figure 3 Snapshots of molecular dynamics simulations. The simulations are for the system forsterite-8,000 atom $MgSiO_3$ liquid perpendicular to the forsterite *a*-axis at various temperatures. The red, blue, and orange spheres represent O, Si, and Mg atoms, respectively.

pressure derivative of the bulk modulus, K', are obtained by fitting the simulated compression results along the third-order Birch-Murnaghan equation of state. The calculated lattice parameters and compressibility show good agreement with the experimental data (Fujino et al. 1981; Duffy et al. 1995; Morimoto and Koto 1969; Angel and Hugh-Jones 1994). We also simulated the bulk $MgSiO_3$ liquid ($N = 8{,}000$) at ambient pressure to verify our inter-atomic potential model by comparing the self-diffusion coefficients of oxygen with other force fields and Car-Parrinello molecular dynamics (de Koker et al. 2009; Adjaoud et al. 2011; Lacks et al. 2007). The calculated diffusion coefficients show good agreement with other molecular dynamics studies (Figure 2a). Figure 2b shows the calculated viscosity using the Einstein-Stokes relation with the effective

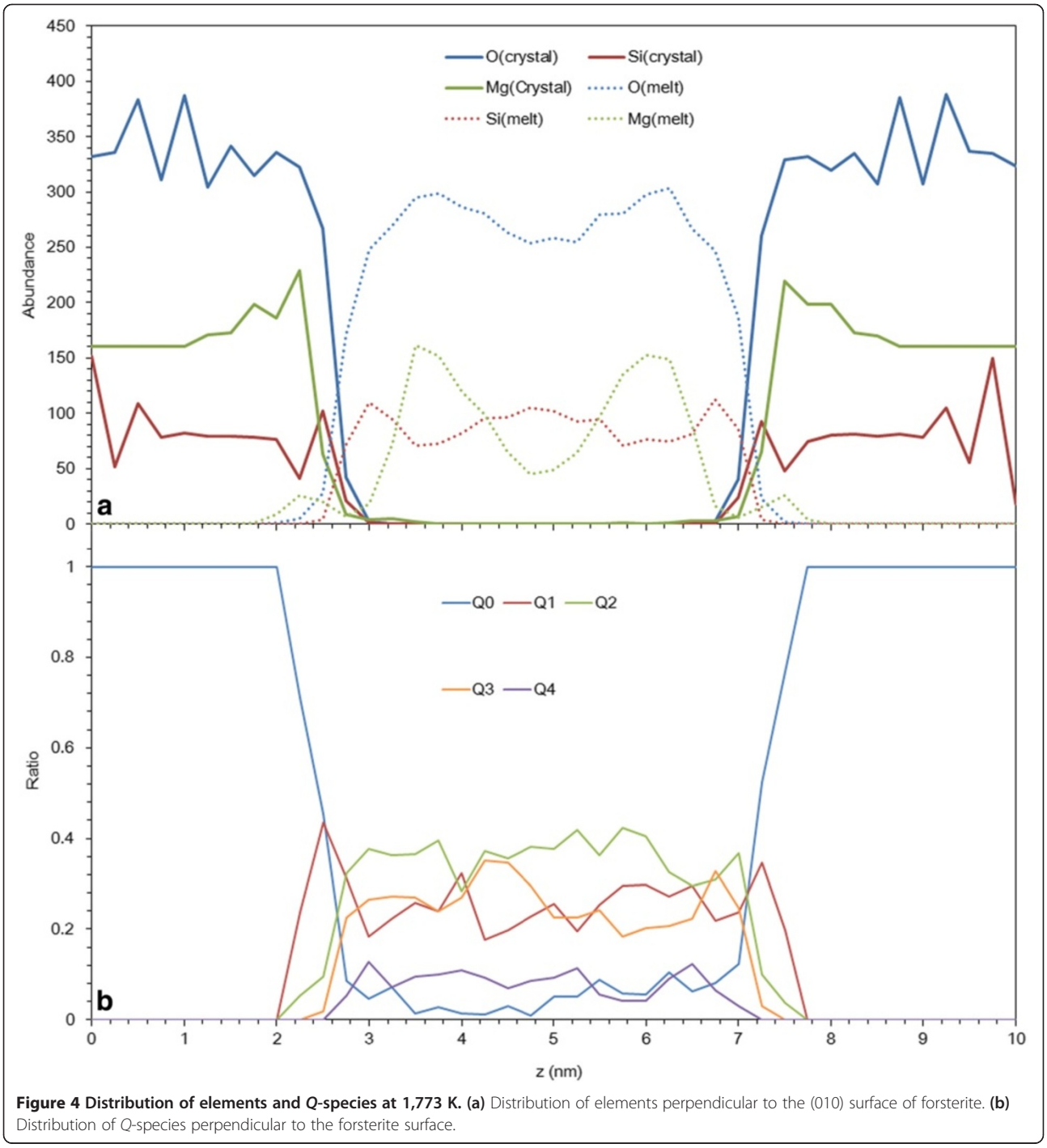

Figure 4 Distribution of elements and *Q*-species at 1,773 K. (a) Distribution of elements perpendicular to the (010) surface of forsterite. **(b)** Distribution of *Q*-species perpendicular to the forsterite surface.

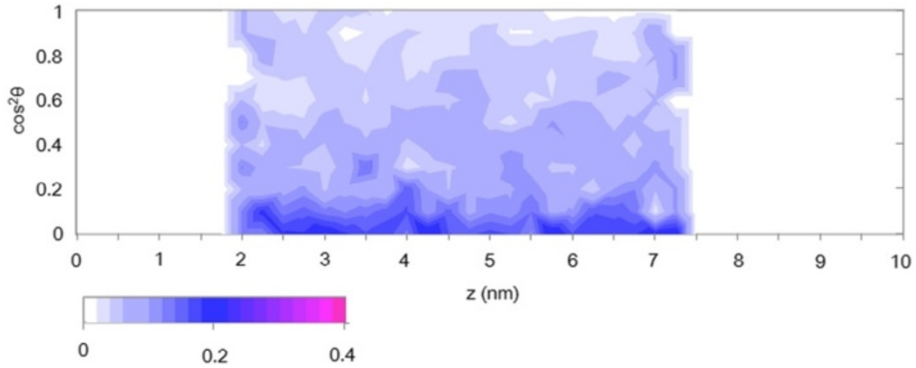

Figure 5 Distribution of the direction of Si-O-Si bridging perpendicular to the forsterite surface. The directions are shown as the $\cos^2\theta$ of the Si-Si vector and *z*-axis.

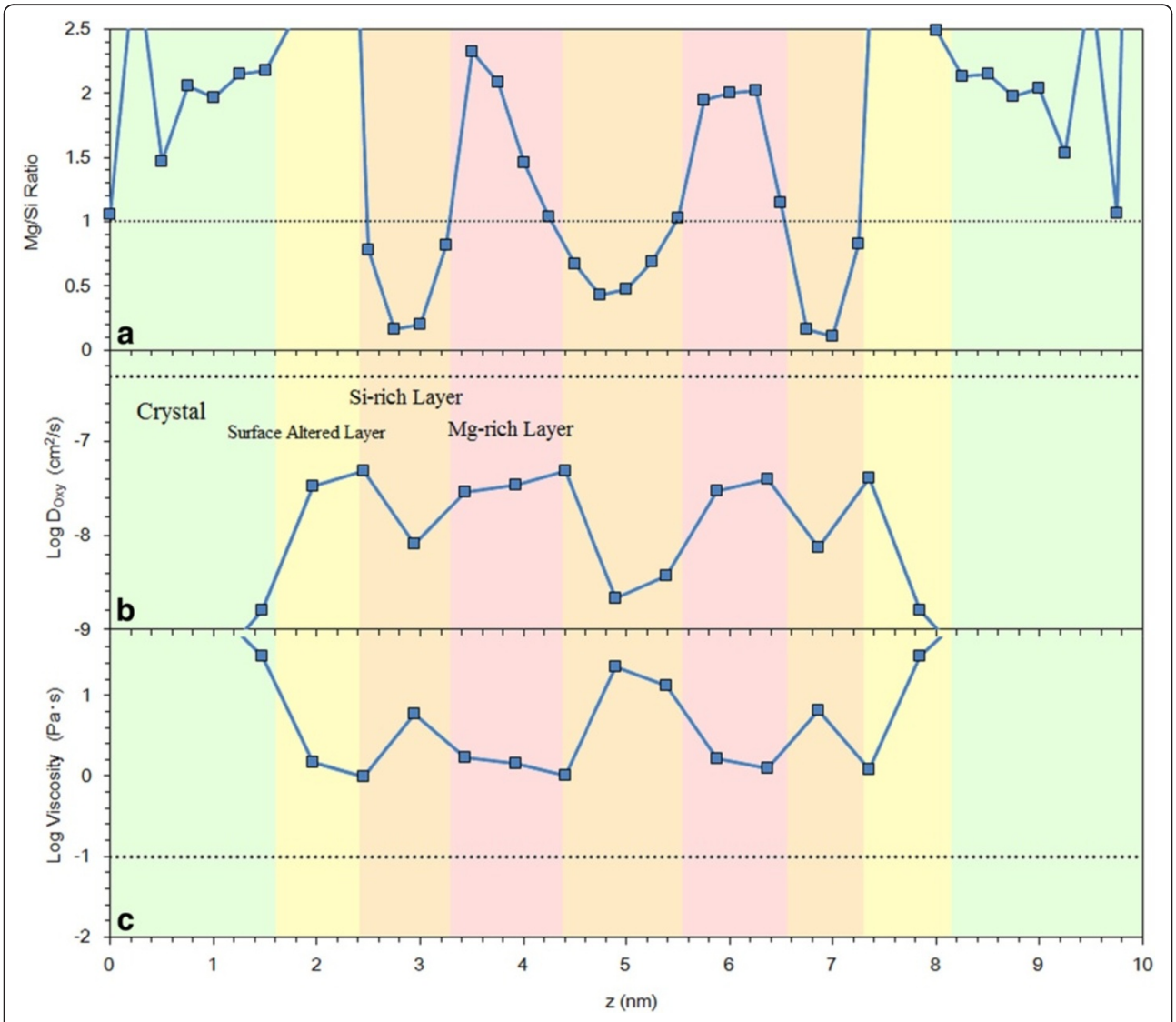

Figure 6 Distribution of Mg/Si ratios, self-diffusion coefficients of oxygen, and viscosities at 1,773 K. (a) Distribution of Mg/Si ratios perpendicular to the (010) surface of forsterite. **(b)** Distribution of two-dimensional self-diffusion coefficients of oxygen parallel to the forsterite surface. **(c)** Distribution of viscosities. The dotted line represents the value of bulk $MgSiO_3$ liquid.

radius reported by Lacks et al. (2007). The viscosity is lower than the experimental data (Bockris et al. 1955) by approximately half an order of magnitude. However, the activation enthalpy shows good agreement with the experimental data.

Results and discussion

4-nm liquid film: the structuralized liquid film

Figure 3 shows snapshots of molecular dynamics simulations perpendicular to the *a*-axis of forsterite using the visualization software VESTA (Momma and Izumi 2011). The liquidus temperature appears to be 1,873 K in Figure 3 because the crystal structure of the forsterite is altered. However, equilibrium is not achieved in a 4.5-ns run at 1,873 K (Figure 1c). The liquidus temperature of the simulated system is approximately 150 K lower than expected from the phase diagram (Jung et al. 2004). Figure 4a shows a distribution of elements perpendicular to the (010) surface of forsterite at 1,773 K. Figure 4b gives a distribution of *Q*-species of Si atoms perpendicular to the forsterite surface at 1,773 K. The threshold length of Si-O bonding for calculating the *Q*-speciation is 0.22 nm. The altered crystal surfaces exist at $z = 2$ to 2.5 nm and 7 to 7.5 nm. The abundance of Mg atoms is higher than that of Si atoms in this region. The nesosilicate structure is disturbed, and 20% to 40% of the SiO_4 tetrahedra form Si-O-Si bridging in this region. In the near crystal surface, the Si-rich layer exists in the liquid domain. The Mg-rich layer exists on the inside of Si-rich layer. Figure 5 shows a distribution of the direction of the Si-O-Si bridging perpendicular to the forsterite surface as a square of the cosine between the *z*-axis and the vector Si-Si calculated as an inner product. The orientation of the Si-O-Si bridging in the sandwiched liquid film is clearly parallel to the crystal surface. Figure 6b gives a distribution of the two-dimensional self-diffusion coefficients of oxygen parallel to the forsterite surface, and Figure 6c shows the calculated viscosities determined using the Einstein-Stokes relation with the effective radius obtained by Lacks et al. (2007). The two-dimensional self-diffusion coefficients of oxygen are consistently lower than that of the bulk $MgSiO_3$ liquid (dotted line) by an order of magnitude. The two-dimensional self-diffusion coefficients of oxygen are strongly related to the Mg/Si ratio of the layer to which the oxygen atoms belong (Figure 6a). In the high Mg/Si ratio layer, the self-diffusion coefficients of oxygen show higher values than those in the low Mg/Si ratio layer.

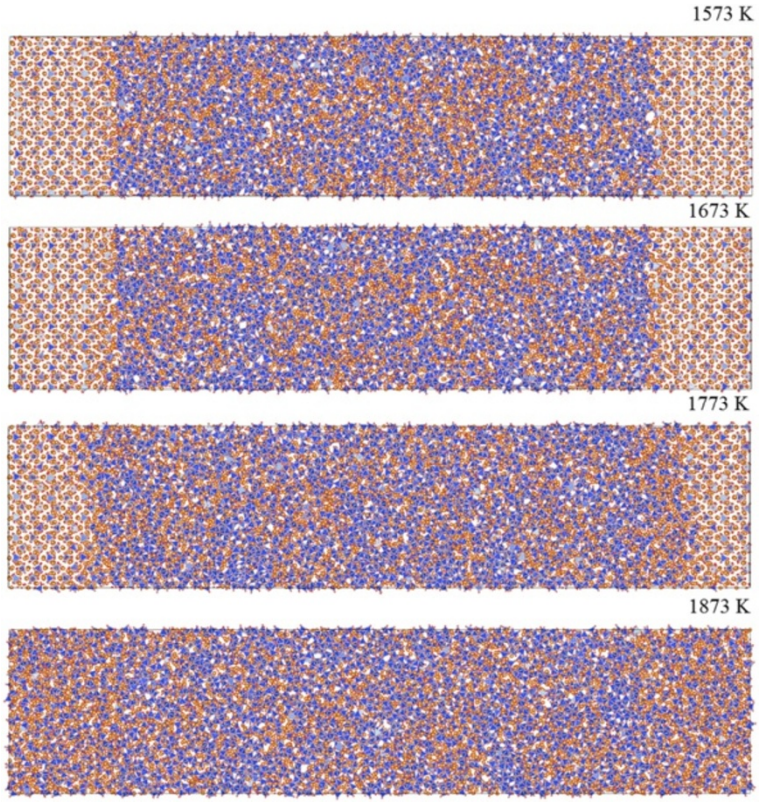

Figure 7 Snapshots of molecular dynamics simulations. Simulations are for the system forsterite-30,000 atom $MgSiO_3$ liquid perpendicular to the *a*-axis of forsterite at various temperatures. The red, blue, and orange spheres represent O, Si, and Mg atoms, respectively.

16-nm liquid film

Figure 7 shows snapshots of molecular dynamics simulations perpendicular to the *a*-axis of forsterite. The volume of the melting part increased at 1,773 K, and the system is completely melted at 1,873 K. Figure 8a shows the distribution of elements perpendicular to the (010) surface of forsterite at 1,673 K. Figure 8b gives the distribution of *Q*-species perpendicular to the forsterite surface at 1,673 K. The altered crystal surfaces exist at z = approximately 3 and 20 nm. The nesosilicate structure is altered, and approximately 20% of the SiO_4 tetrahedra formed Si-O-Si bridging in this region. In the near crystal surface, the Si-rich layer exists in the liquid domain. In the domain between the disturbed crystal surface and the Si-rich layer, Si-O-Si bridging is formed, and Q^1 becomes the dominant species. The Mg-rich layer exists on the inside of the Si-rich layer. The composition of the sliced layer of the $MgSiO_3$ liquid is heterogeneous and oscillates, whereas the sliced layer is distant from the crystal surface (Figure 8a). Figure 9 shows the distribution of the direction of the Si-O-Si bridging perpendicular to the forsterite surface. The orientation of the Si-O-Si bridging in the sandwiched liquid film is clearly parallel to the crystal surface. However, the orientation in the disturbed crystal surface is strongly perpendicular to the crystal surface. Figure 10b gives the distribution of two-dimensional self-diffusion coefficients of oxygen parallel to the forsterite surface, and Figure 10c shows the calculated viscosities. The two-dimensional self-diffusion coefficients of oxygen are all slightly lower than those of bulk $MgSiO_3$ liquids (dotted line). The two-dimensional self-diffusion coefficients of oxygen are strongly related to the Mg/Si ratio of each layer in which the oxygen atoms belong in the liquid region. In the high Mg/Si ratio layers, the self-diffusion coefficients of oxygen show larger values than in the low Mg/Si ratio layers (Figure 10a). However, coefficients in altered crystal surface regions are lower than those in liquid regions, in contrast to the case of the 4-nm liquid film.

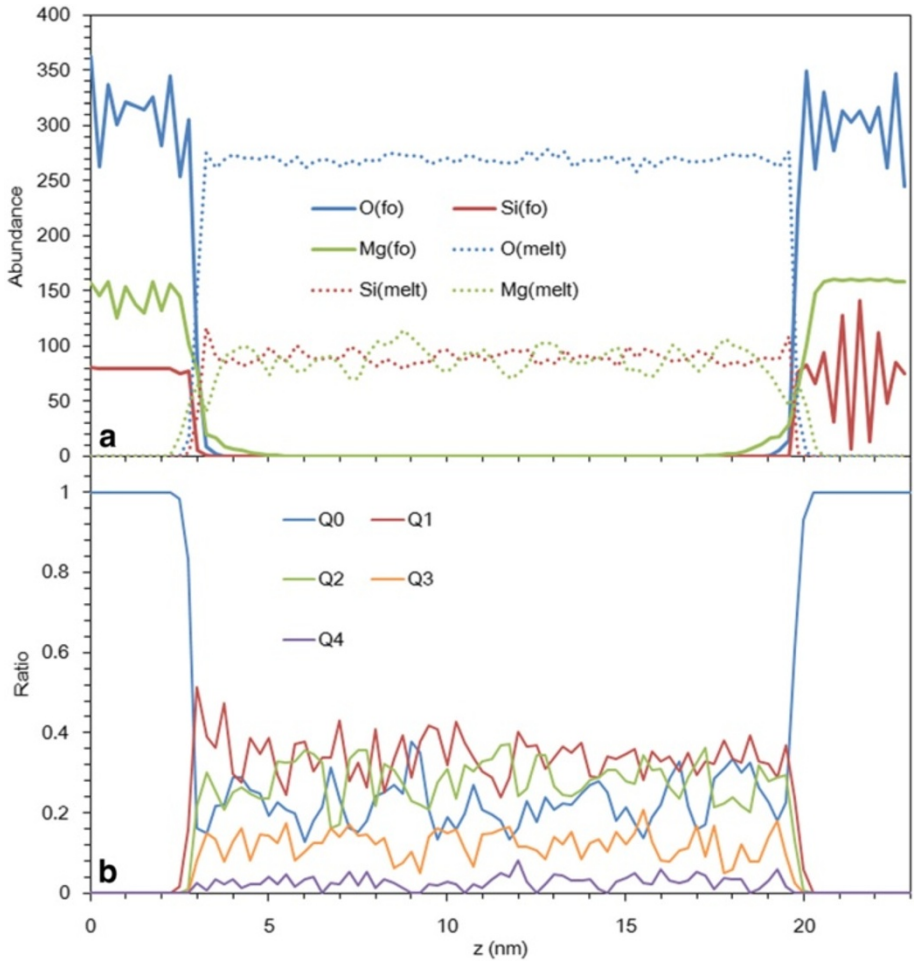

Figure 8 Distribution of elements and *Q*-species at 1,673 K. (a) Distribution of elements perpendicular to the (010) surface of forsterite. **(b)** Distribution of *Q*-species perpendicular to the forsterite surface.

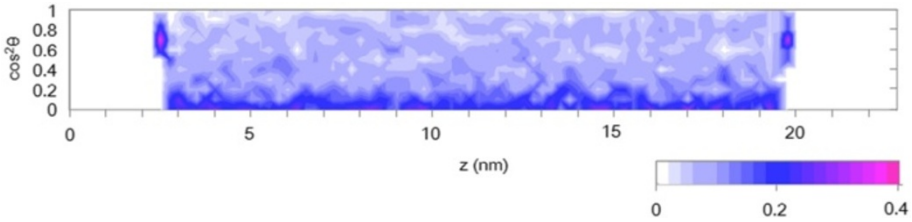

Figure 9 Distribution of the direction of the Si-O-Si bridging perpendicular to the forsterite (010) surface. The directions are shown as the $\cos^2\theta$ of the Si-Si vector and *z*-axis.

Effect of film thickness

We show the result of simulation of the system containing films of 7- and 28-nm thickness. The layered structure is also found in this system. However, the global decrease of self-diffusion coefficients is much smaller than the interface system with the 4-nm liquid film (Figure 11). Figure 12 shows the distribution of the Mg/Si ratio, elements, and the two-dimensional self-diffusion coefficients of oxygen of the system with a 28-nm liquid film. The layered structure is similar to the case of the 16-nm liquid film. The two-dimensional self-diffusion coefficients of oxygen in the middle part ($z = 12$ to 23 nm) of the liquid films are the same as those of bulk liquids. This means that the $MgSiO_3$ liquid film sandwiched by the forsterite (010) surface acts like a bulk liquid in the region 7 nm apart from the crystal surface. Figure 13 shows the calculated

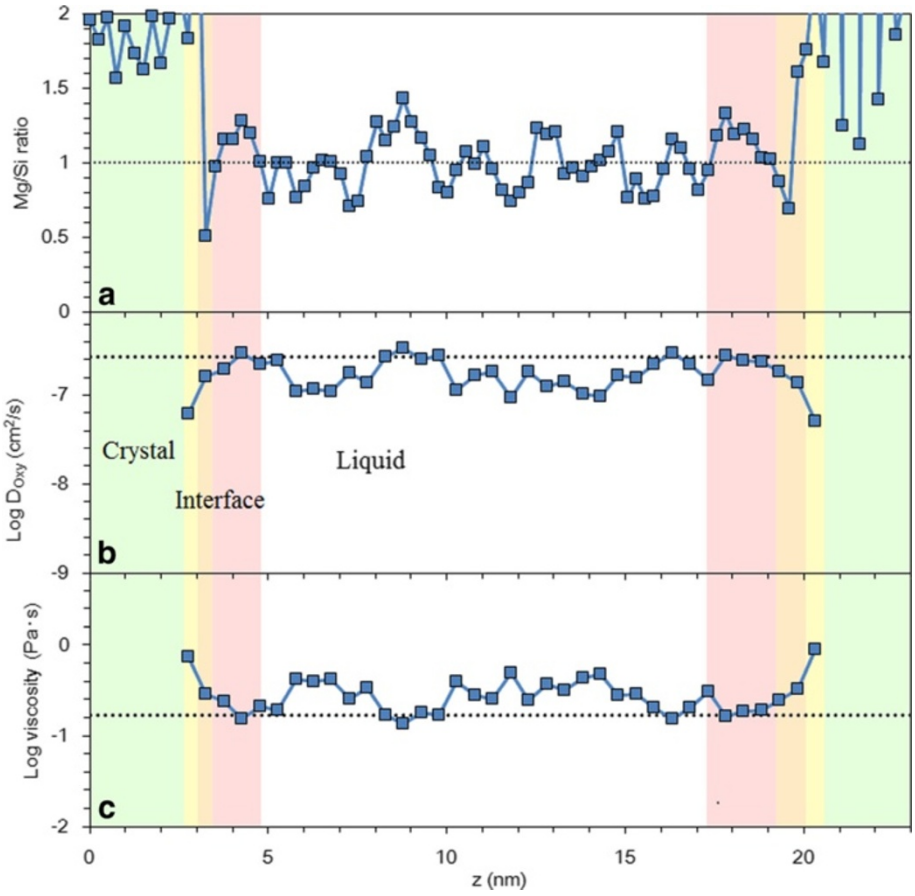

Figure 10 Distribution of Mg/Si ratios, self-diffusion coefficients of oxygen, and viscosities at 1,673 K. (a) Distribution of Mg/Si ratio perpendicular to the (010) surface of forsterite. **(b)** Distribution of two-dimensional self-diffusion coefficients of oxygen parallel to the forsterite surface. **(c)** Distribution of viscosities. The dotted line represents the value of bulk $MgSiO_3$ liquid.

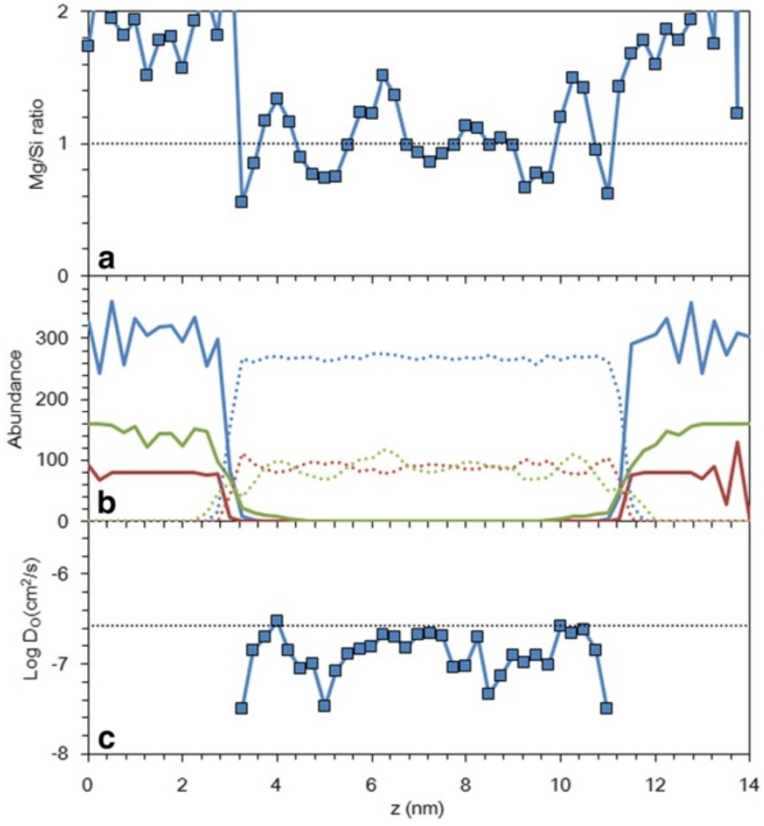

Figure 11 Mg/Si ratios, elements, and self-diffusion coefficients of oxygen for forsterite-$MgSiO_3$ with 7-nm liquid film. (a) Distribution of Mg/Si ratio perpendicular to the (010) surface of forsterite at 1,673 K. **(b)** Distribution of elements perpendicular to the (010) surface of forsterite at 1,673 K. **(c)** Distribution of two-dimensional self-diffusion coefficients of oxygen parallel to the forsterite surface at 1,673 K.

viscosities for various film thicknesses. The average viscosity approaches the viscosity of a bulk liquid with increasing film thickness. The average viscosity in the liquid films of 28-nm thickness is nearly the same as that of a bulk liquid. The average viscosity in the thin (<5 nm) liquid film is much higher than that of a bulk liquid.

General discussion

The layered structure that exists in the liquid films in these simulations is caused by the difference in bond strength between Si-O semi-covalent bonds and Mg-O ionic bonds. Si-O-Si bridgings are excessively formed between the altered crystal surface and the Si-rich layer because the strength of Si-O bonding is much higher than that of Mg-O bonding. The excess formation of Si-O-Si bridging in these compositions produce free oxygen atoms. Formation of Si-O-Si bridging depletes the non-bridging oxygen as an acceptor of magnesium atoms and concentrates silicon atoms. The excess free oxygen atoms concentrate magnesium atoms. Consequently, an Si-rich layer is formed in the nearest surface region of the liquid domain, and an Mg-rich layer is formed on the inside of the Si-rich layer on the liquid film (Figures 6a and 10a). The *Q*-speciation reflects the Mg/Si ratio on the Si-rich layer because Q^4 species increase in the case of the 4-nm liquid film. However, the *Q*-speciation does not reflect the Mg-rich layer. The abundance of Q^0 is too small in the case of the 4-nm film (Figure 4), meaning free oxygen atoms are produced. Clustering of the -Si-O- network also occurs. The *Q*-speciation does not reflect the Mg/Si ratio because the -Si-O- corner shared network makes the cluster. The clustering and layering weaken with increasing film thickness. The weakening can be explained by the degree of freedom in the film structure. The excess free oxygen and magnesium atoms from altered surfaces could not be accepted in the liquid film in the case of a thin film because the degree of freedom in the film structure is small. However, they can be accepted in a liquid film with increasing film thickness. Consequently, the degree of clustering decreases with increasing film thickness (Figures 6, 10, 11 and 12).

The layered structure is also reported by Gurmani et al. (2011). They investigated forsterite-$MgSiO_3$ liquid with a film thickness of up to 8 nm by the classical molecular dynamics method. However, the contrast of

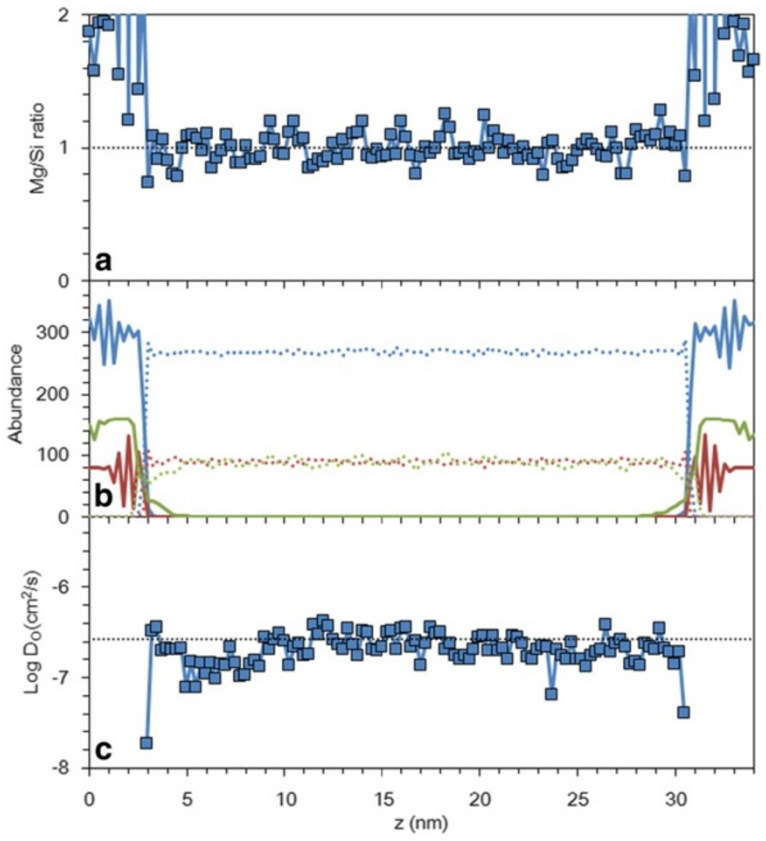

Figure 12 Mg/Si ratios, elements, and self-diffusion coefficients of oxygen for forsterite-$MgSiO_3$ with 28-nm liquid film. (a) Distribution of Mg/Si ratio perpendicular to the (010) surface of forsterite at 1,673 K. **(b)** Distribution of elements perpendicular to the (010) surface of forsterite at 1,673 K. **(c)** Distribution of two-dimensional self-diffusion coefficients of oxygen parallel to the forsterite surface at 1,673 K.

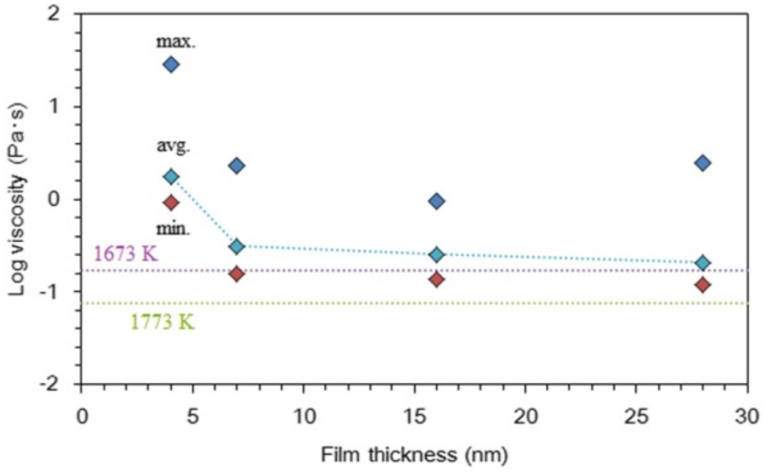

Figure 13 Plots of viscosity as a function of film thickness. Max. and min. denote the maximum and minimum viscosity in the liquid region, respectively. Avg. means the average of the entire liquid film (4 and 7 nm) and the average of the region 5 nm apart from the crystal surface (16 and 28 nm).

composition and decrease of self-diffusion coefficients by the interface was much smaller than in our study. The difference between Gurmani et al. (2011) and our studies is caused by the area of the surface cross section. Horbach et al. (1996) reported the finite-size effects in simulations of silicate glass. According to their study, the system should contain more than 8,000 atoms (4 to 5 nm for each side of the periodic cell) to avoid the size effects. Gurmani et al. (2011) simulated the same system with approximately 2-nm length sides for the cross section of the interface. The length of the cross section of our simulation is approximately 5 nm to avoid the size effects reported by Horbach et al. (1996).

The structure of the altered crystal surface seems to be different because of the thickness of the liquid films. The concentration of magnesium in the altered crystal surface with the 4-nm liquid film is much higher than that with the 16-nm liquid film (Figures 4a and 8a). In addition, the orientation of Si-O-Si bridging in the altered crystal surface with the 16-nm liquid film is strongly perpendicular to the crystal surface compared with the surface with the 4-nm liquid film (Figures 5 and 9). These differences might be explained by the degree of freedom of the configuration of the liquid films. There might be no structural flexibility in the liquid domain to accept the excess magnesium atoms in altered crystal surfaces because there are only five layers in the 4-nm liquid film. In contrast, the concentration of magnesium in the altered crystal surface with the 16-nm liquid film is lower than that with the 4-nm liquid film because of the structural flexibility of the liquid film. The surface becomes well-ordered by acceptation of magnesium in liquid and disordered by existence of excess magnesium atoms.

The two-dimensional self-diffusion coefficients parallel to the crystal surface are dependent on their distance from the altered crystal surface. Those coefficients show larger values in Mg-rich layers and smaller values in Si-rich layers. The regional dependences are simply explained by the composition of the sliced layer. Self-diffusion coefficients of network-forming elements in binary silicate liquids depend on their SiO_2 contents (Keller et al. 1982; Keller and Schwerdtfeger 1979). Self-diffusion coefficients of Si and O atoms decrease with increasing SiO_2 contents in bulk silicate liquids because of the difference in bond strength between Si-O covalent bonds and ionic bonds. Consequently, the self-diffusion coefficients of oxygen atoms decrease in Si-rich layers and increase in Mg-rich layers. The two-dimensional self-diffusion coefficients of oxygen in the 4-nm liquid film are lower than those in the 16-nm liquid film by an order of magnitude (Figures 4b and 8b). The difference in the self-diffusion coefficients might be explained by the structural flexibility of liquid films. The variety of Mg/Si ratios in the 4-nm liquid film is larger than that in the 16-nm liquid film. The degree of freedom of the configuration in the 4-nm liquid film is lower than that in the 16-nm liquid film. The liquid film is strongly structured by the crystal surface in the case of thin liquid films. Consequently, the flexibility of motion of each atom in the 4-nm liquid film is lower than that in the 16-nm liquid film, and mobility is decreased by the lower flexibility.

The oxygen diffusivity is related to shear viscosity by the Einstein-Stokes relation. The Einstein-Stokes relation is stated as

$$D = kT/6\pi r\eta, \tag{4}$$

where D is the self-diffusion coefficient, k is the Boltzmann constant, T is the temperature, r is the radius of diffusing particles, and η is the shear viscosity. This equation has been used with remarkable success in a variety of silicate liquids to relate diffusivity of network forming atoms and shear viscosity (e.g., Oishi et al. 1975; Dunn 1982; Shimizu and Kushiro 1984; Rubie et al. 1993; Lacks et al. 2007). Applying the Einstein-Stokes relation to the results of this study, the viscosity of thin film silicate liquid might be considered to have higher viscosity than bulk liquid by 1 order of magnitude (Figure 6c). In the 16-nm film liquid, the viscosity of the liquid is slightly lower than that of bulk liquid in the near surface region, the same as with bulk liquid in the Mg-rich layer, and oscillates with distance from the crystal surface (Figure 10c).

Implications

The melt segregation velocity in partially molten rock is inversely proportional to the melt viscosity (McKenzie 1989). In texturally equilibrated partially molten rocks, melts reside at the grain corners and edges (see Figure one of Zhu and Hirth 2003). A melt channel exists on the grain edge, and its cross-sectional area is determined by the dihedral angle, the melt fraction, and grain size. Von Bargen and Waff (1986) showed that the minimum channel cross-sectional area of partially molten rock consists of tetrakaidecahedron grains of varying melt fraction and dihedral angle θ. We calculated the viscosity at melt channels using the results of our simulations (Figure 13) and geometrical calculation by von Bargen and Waff (1986). Figure 14 shows the logarithm of normalized viscosity of melts in melt channels versus melt fraction with two grain sizes and two dihedral angles. Waff and Bulau (1979) showed that the distribution of dihedral angles in partially molten ultramafic rocks is between 30° and 47°. The viscosity becomes higher than bulk liquids by 1 order of magnitude at lower melt fractions and 1-μm grain. However, viscosity seems to be constant with varying melt fractions in the case of 10-μm grain size. The

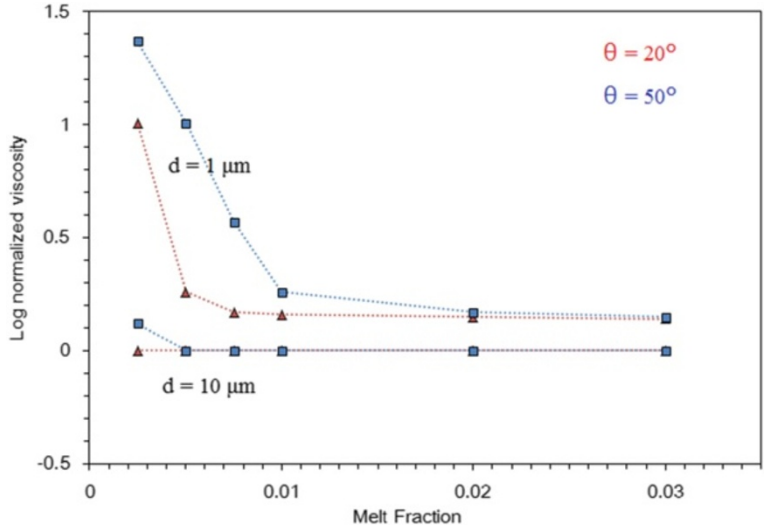

Figure 14 Plots of normalized viscosity at melt channels as a function of melt fraction. *d* and *θ* in the figure mean grain size and dihedral angle, respectively.

effect of the silicate crystal-liquid interface is negligible in melt flow in the mantle conditions, postulating the textural equilibrium, because the range in grain size of the mantle is 1 to 50 mm (Faul and Jackson 2005). However, a melt film of 0.6- to 3.0-nm thickness was found in deformed partially molten olivine-orthopyroxene rocks (de Kloe et al. 2000). Consequently, the crystal-liquid interface can affect the melt flow in deformed samples.

Conclusions

We showed the results of molecular dynamics simulations of forsterite-$MgSiO_3$ liquid, which contribute to our understanding of the nanoscale structure of the interface and diffusivity of atoms in the interface. From these simulations, the characteristic structure of liquid films in forsterite-$MgSiO_3$ liquid interface is observed. We also observe the layered structure of an altered crystal surface, an Si-rich layer, and an Mg-rich layer in the crystal-liquid interface. The layered structure is formed by the strength difference between Si-O covalent bonds and Mg-O ionic bonds. Si-O-Si bridging and free oxygen atoms are excessively formed in the near surface because Si-O bonding is much stronger than Mg-O bonding. The difference in the layered structure indicated by the thickness of $MgSiO_3$ liquid films might be caused by the difference in degree of freedom of the configuration in liquid films. The two-dimensional diffusivity of oxygen is controlled by two factors. One factor is the thickness of the liquid films that decreases oxygen diffusivity with decreasing film thickness because of the decrease of degree of freedom of the configuration in the liquid films. The other factor is the composition of the sliced layer, where oxygen diffusivity increases with increasing Mg/Si ratio because Si-O bonding is much stronger than Mg-O bonding. The degree of Mg/Si layering strongly depends on film thickness and decreases with increasing film thickness. The effect of the crystal-liquid interface is negligible in texturally equilibrated rocks. However, the interface can affect the melt flow in deformed samples because the grain boundary melt film of several nanometer thickness exists stably in deformed partially molten rocks.

Competing interests

The authors declare that they have no competing interests.

Authors' contributions

FN performed the simulations and analyzed the data. Both FN and KK proposed the topic, designed the study, mutually discussed throughout the study, and wrote the paper. Both authors read and approved the final manuscript.

Acknowledgements

We thank the editor and three anonymous reviewers for the valuable comments. This work was supported by the Grant-in-Aid for JSPS fellows, 251856.

Received: 14 March 2014 Accepted: 25 May 2014
Published: 20 June 2014

References

Adjaoud O, Steinle-Neumann G, Jahn S (2011) Transport properties of Mg_2SiO_4 liquid at high pressure: physical state of magma ocean. Earth Planet Sci Lett 312:463–470, doi:10.1016/j.epsl.2011.10.025

Angel RJ, Hugh-Jones DA (1994) Equations of state and thermodynamic properties of enstatite pyroxenes. J Geophys Res 99:19777–19783, doi:10.1029/94JB01750

Bockris JO'M, Mackenzie JD, Kitchener JA (1955) Viscous flow in silica and binary liquid silicates. Trans Faraday Soc 51:1734–1748, doi:10.1039/TF9555101734

De Kloe R, Drury MR, van Roermund HLM (2000) Evidence for stable grain boundary melt films in experimentally deformed olivine-orthopyroxene rocks. Phys Chem Min 27:480–494, doi:10.1007/s002690000090

De Koker NP, Stixrude L, Karki B (2009) Thermodynamics, structure, dynamics, and freezing of Mg_2SiO_4 liquid at high pressure. Geochim Cosmochim Acta 72:1427–1441, doi:10.1016/j.gca.2007.12.019

Duffy TS, Zha C, Downs RT, Mao H, Hemley RJ (1995) Elasticity of forsterite to 16 GPa and the composition of the upper mantle. Nature 378:170–173

Dunn T (1982) Oxygen diffusion in three silicate melts along the join diopside-anorthite. Geochim Cosmochim Acta 46:2293–2299, doi:10.1016/0016-7037(82)90202-2

Faul UH, Jackson I (2005) The seismological signature of temperature and grain size variations in the upper mantle. Earth Planet Sci Lett 234:119–134, doi:10.1016/j.epsl.2005.02.008

Fujino K, Sasaki S, Takeuchi Y, Sadanaga R (1981) X-ray determination of electron distributions in forsterite, fayalite and tephroite. Acta Crystallogr B 37:513–518, doi:10.1107/S0567740881003506

Gurmani SF, Jahn S, Brasse H, Schilling FR (2011) Atomic scale view on partially molten rocks: molecular dynamics simulations of melt-wetted olivine grain boundaries. J Geophys Res 116:V12209, doi:10.1029/2011JB008519

Hiraga T, Anderson LM, Zimmerman ME, Mei S, Kohlstedt DL (2002) Structure and chemistry of grain boundaries in deformed, olivine + basalt and partially molten lherzolite aggregates: evidence of melt-free grain boundaries. Contrib Mineral Petrol 144:163–175, doi:10.1007/s00410-002-0394-1

Horbach J, Kob W, Binder K, Angell CA (1996) Finite size effects in simulations of glass dynamics. Phys Rev E 54:R5897–R5900, doi;10.1103/PhysRevE.54.R5897

Ichikawa Y, Kawamura K, Nakano M, Kitayama K, Seiki T, Theramast N (2001) Seepage and consolidation of bentonite saturated with pure- or salt-water by the method of unified molecular dynamics and homogenization analysis. Eng Geol 60:127–138, doi:10.1016/S0013-7952(00)00095-8

Jung I, Decterov SA, Pelton AD (2004) Critical thermodynamic evaluation and optimization of the FeO-Fe_2O_3-MgO-SiO_2 system. Metall Mater Trans B 35:877–889, doi:10.1007/s11663-004-0082-9

Keller H, Schwerdtfeger K (1979) Tracer diffusivity of Si^{31} in CaO-SiO_2 melts at 1600 °C. Metall Trans B 10:551–554

Keller H, Schwerdtfeger K, Petri H, Hölzle R, Hennesen K (1982) Tracer diffusivity of O^{18} in CaO-SiO_2 melts at 1600 °C. Metall Trans B 13:237–240

Lacks DJ, Rear DB, van Orman JA (2007) Molecular dynamics investigation of viscosity, chemical diffusivities and partial molar volumes of liquids along the MgO-SiO_2 join as functions of pressure. Geochim Cosmochim Acta 71:1312–1323, doi:10.1016/j.gca.2006.11.030

McKenzie D (1989) Some remarks on the movement of small melt fractions in the mantle. Earth Planet Sci Lett 95:53–72, doi:10.1016/0012-821X(89)90167-2

Momma K, Izumi F (2011) VESTA 3 for three-dimensional visualization of crystal, volumetric and morphology data. J Appl Crystallogr 44:1272–1276, doi:10.1107/S0021889811038970

Morimoto N, Koto K (1969) The crystal structure of orthoenstatite. Z Kristallogr – Cryst Mater 129:65–83

Noritake F, Kawamura K, Yoshino T, Takahashi E (2012) Molecular dynamics simulation and electrical conductivity measurement of $Na_2O \cdot 3SiO_2$ melt under high pressure; relationship between its structure and properties. J Non-Cryst Solids 358:3109–3118, doi:10.1016/j.noncrysol.2012.08.027

Oishi Y, Terai R, Ueda H (1975) Oxygen diffusion in liquid silicates and relation to their viscosity. In: Cooper A (ed) Mass transport phenomena in ceramics. Material science research, vol 9. Springer, New York, pp 297–310

Rubie DC, Ross CR, Carroll MR, Elphick SC (1993) Oxygen self-diffusion in $Na_2Si_4O_9$ liquid up to 10 GPa and estimation of high-pressure melt viscosities. Am Mineral 78:574–582

Sakuma H, Kawamura K (2009) Structure and dynamics of water on muscovite mica surfaces. Geochim Cosmochim Acta 73:4100–4110, doi:10.1016/j.gca.2009.05.029

Sakuma H, Tsuchiya T, Kawamura K, Otsuki K (2003) Large self-diffusion of water on brucite surface by ab initio potential energy surface and molecular dynamics simulations. Surf Sci 536:L396–L402, doi:10.1016/S0039-6028(03)00577-6

Shimizu N, Kushiro I (1984) Diffusivity of oxygen in jadeite and diopside melts at high pressures. Geochim Cosmochim Acta 48:1295–1303, doi:10.1016/0016-7037(84)90063-2

Von Bargen N, Waff HS (1986) Permiabilities, interfacial areas and curvatures of partially molten systems: results of numerical computations of equilibrium microstructures. J Geophys Res 91:9261–9276, doi:10.1029/JB091iB09p09261

Waff HS, Bulau JR (1979) Equilibrium fluid distribution in an ultramafic partial melt under hydrostatic stress conditions. J Geophys Res 84:6109–6114, doi:10.1029/JB084iB11p06109

Zhu W, Hirth G (2003) A network model for permeability in partially molten rocks. Earth Planet Sci Lett 212:407–416, doi:10.1016/S0012-821X(03)00264-4

doi:10.1186/2197-4284-1-14
Cite this article as: Noritake and Kawamura: **Structure and properties of forsterite-$MgSiO_3$ liquid interface: molecular dynamics study.** *Progress in Earth and Planetary Science* 2014 **1**:14.